

SCIENTIFIC REPORTS



OPEN

Structural basis for cytokinin production by LOG from *Corynebacterium glutamicum*

Hogyun Seo¹, Sangwoo Kim^{1,2}, Hye-Young Sagong¹, Hyeoncheol Francis Son¹,
Kyeong Sik Jin³, Il-Kwon Kim⁴ & Kyung-Jin Kim¹

Received: 24 March 2016

Accepted: 19 July 2016

Published: 10 August 2016

“Lonely guy” (LOG) has been identified as a cytokinin-producing enzyme in plants and plant-interacting fungi. The gene product of *Cg2612* from the soil-dwelling bacterium *Corynebacterium glutamicum* was annotated as an LDC. However, the facts that *C. glutamicum* lacks an LDC and *Cg2612* has high amino acid similarity with LOG proteins suggest that *Cg2612* is possibly an LOG protein. To investigate the function of *Cg2612*, we determined its crystal structure at a resolution of 2.3 Å. *Cg2612* functions as a dimer and shows an overall structure similar to other known LOGs, such as LOGs from *Arabidopsis thaliana* (AtLOG), *Claviceps purpurea* (CpLOG), and *Mycobacterium marinum* (MmLOG). *Cg2612* also contains a “PGG_xGT_{xx}E” motif that contributes to the formation of an active site similar to other LOGs. Moreover, biochemical studies on *Cg2612* revealed that the protein has phosphoribohydrolase activity but not LDC activity. Based on these structural and biochemical studies, we propose that *Cg2612* is not an LDC family enzyme, but instead belongs to the LOG family. In addition, the prenyl-binding site of *Cg2612* (CgLOG) comprised residues identical to those seen in AtLOG and CpLOG, albeit dissimilar to those in MmLOG. The work provides structural and functional implications for LOG-like proteins from other microorganisms.

The term cytokinin originated from the cell division-promoting functions of these compounds¹. Cytokinin phytohormones are usually N⁶-modified adenines such as N⁶-(δ^2 -isopentenyl)adenine (iP) and trans-zeatin (tZ), and they play significant roles in controlling growth and development of plants^{2,3}. They can be conjugated with sugar moieties such as nucleotides, nucleosides, and glucosides, but these conjugated forms are biologically less active or inactive for plant cytokinin receptors². The cytokinin biosynthetic pathway begins with dimethylallyl pyrophosphate (DMAPP), possibly originating from the mevalonate or methylerythritol phosphate pathway, being prenylated by isopentenyltransferase (IPT) (Fig. 1a). Adenylate-IPT can add DMAPP to ATP/ADP or adenylate, whereas tRNA-IPT modifies the N⁶-atom of adenine moiety on position 37 of tRNA⁴. The isopentenylated products can be converted to the typical metabolite N-(δ -isopentenyl)adenosine 5'-monophosphate (iPRMP) by dephosphorylation or degradation of tRNA⁵. The nucleotide iPRMP might be dephosphorylated by nucleotidase and then deribosylated by nucleosidase to produce an active nucleobase². In 2007, a one-step cytokinin activation pathway was first discovered and the novel cytokinin-activating enzyme called lonely guy (LOG) emerged⁶. LOG produces active cytokinins via dephosphoribosylation, directly hydrolyzing the bond between N⁶-substituted bases and ribose 5'-monophosphates in cytokinin precursors such as iPRMP or trans-zeatin riboside 5'-monophosphate (tZRMP).

For many years, before the discovery of their cytokinin-producing activity, LOGs were known as possible lysine decarboxylases (LDCs) according to the Pfam database, without experimental evidence⁷. Recently, enzymes from several organisms, such as *Oryza sativa*, *Arabidopsis thaliana*, *Claviceps purpurea*, and *Mycobacterium tuberculosis* have been identified as LOGs by biochemical and functional studies^{5,6,8,9}. According to morphological and metabolic analyses, the LOG-mediated one-step pathway is suggested as the major cytokinin production pathway and is pivotal for normal growth and development in *Arabidopsis*⁸. Despite a lack of evidence for the phosphoribohydrolase catalytic mechanism, the homodimeric disposition and the active site with highly conserved

¹School of Life Sciences, KNU Creative BioResearch Group, Kyungpook National University, Daegu 702-701, Republic of Korea. ²School of Nano-Bioscience and Chemical Engineering, Ulsan National Institute of Science and Technology (UNIST), Ulsan, 689-798, Republic of Korea. ³Pohang Accelerator Laboratory, Pohang University of Science and Technology, Jigok-ro 80, Pohang, Kyungbuk 790-784, Korea. ⁴Bioprocess Research Depart. R&D Center, DAESANG Corp., Icheon-si, Gyeonggi-do, 467-810, Republic of Korea. Correspondence and requests for materials should be addressed to K.-J.K. (email: kkim@knu.ac.kr)

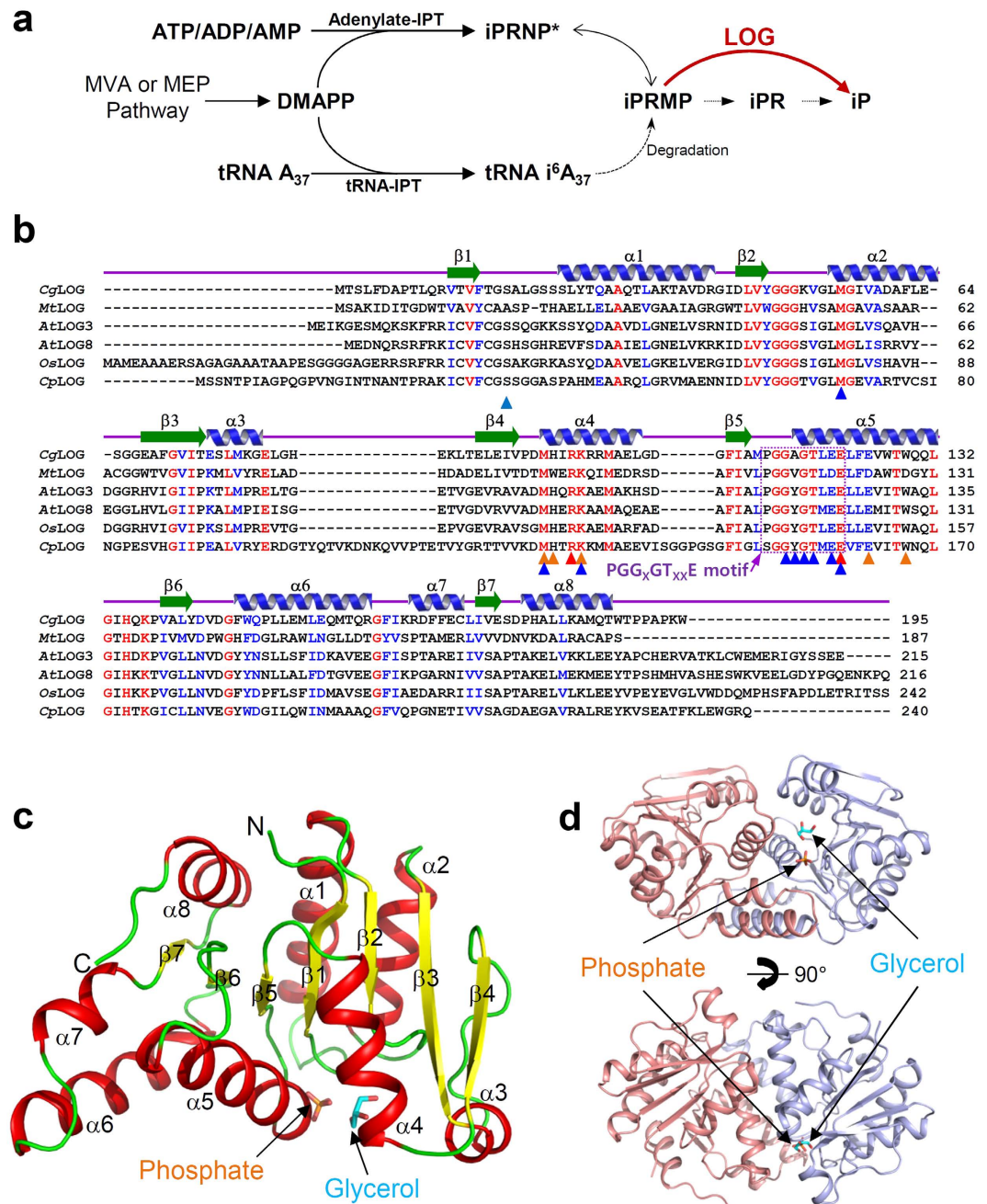


Figure 1. Overall structure of CgLOG. (a) Biosynthetic pathway for cytokinin production. (b) Amino acid sequence alignment of LOGs. The secondary structure elements are drawn based on the structure of CgLOG. Residues involved in catalysis, AMP binding, and prenyl-group binding are indicated by red, blue, and orange-colored triangles, respectively. The PGG_xGT_{xx}E motif is indicated with a purple-colored dotted rectangle. CgLOG, MtLOG, AtLOG, OsLOG, and CpLOG are abbreviations of LOGs from *Corynebacterium glutamicum*, *Mycobacterium tuberculosis*, *Arabidopsis thaliana*, *Oryza sativa*, and *Claviceps purpurea*, respectively. (c) The monomeric structure of CgLOG presented as a cartoon diagram. The bound glycerol and phosphate molecules are shown as stick models. Secondary structure elements are labeled. (d) Dimeric structure of CgLOG. The dimeric structure of CgLOG is presented as a cartoon diagram. The bound glycerol and phosphate molecules are shown as in (c). The bottom figure is the top figure rotated horizontally by 90°.

“PGG_xGT_{xx}E” motif were elucidated by structural studies on LOG proteins^{10,11}. However, many LOG-like proteins, especially from bacteria, have remained *terra incognita*.

The soil-dwelling bacterium *Corynebacterium glutamicum* has been intensively studied for industrial applications due to its high production of amino acids, nucleotides, and vitamins¹². Among these products, L-lysine has most actively drawn attention in industry¹³. Interestingly, *C. glutamicum* ATCC 13032 contains a gene product

CgLOG	
Data collection	
Space group	I222
Cell dimensions	
<i>a</i> , <i>b</i> , <i>c</i> (Å)	113.5, 130.5, 140.5
α , β , γ (°)	90.00, 90.00, 90.00
Resolution (Å)	50.00–2.30 (2.34–2.30)
R_{sym} or R_{merge}	10.2 (31.9)
$I/\sigma I$	17.5 (3.5)
CC1/2	0.989 (0.63)
Completeness (%)	95.2 (87)
Redundancy	6.8 (3.2)
Refinement	
Resolution (Å)	50.00–2.30
No. reflections	41951
$R_{\text{work}}/R_{\text{free}}$	18.3/23.0
No. atoms	6149
Protein	5899
Glycerol/ PO_4^{3-}	36/10
Water	204
<i>B</i> -factors	29.69
Protein	29.76
Glycerol/ PO_4^{3-}	38.04/20.20
Water	30.13
R.m.s. deviations	
Bond lengths (Å)	0.015
Bond angles (°)	1.704

Table 1. Data collection and structural refinement statistics. ^aThe numbers in parentheses are statistics from the highest resolution shell. ^b $R_{\text{sym}} = \sum |I_{\text{obs}} - I_{\text{avg}}|/I_{\text{obs}}$, where I_{obs} is the observed intensity of individual reflection and I_{avg} is average over symmetry equivalents. ^c $R_{\text{work}} = \sum ||F_{\text{o}}| - |F_{\text{c}}||/\sum |F_{\text{o}}|$, where $|F_{\text{o}}|$ and $|F_{\text{c}}|$ are the observed and calculated structure factor amplitudes, respectively. R_{free} was calculated with 5% of the data.

of Cg2612 that is annotated as a possible LDC (pfam03641) and a nucleotide-binding protein. LDCs are known as pyridoxal 5'-phosphate (PLP)-dependent enzymes that convert L-lysine to cadaverine by a decarboxylation reaction¹⁴. Ironically, *C. glutamicum* is also known to lack LDC, which results in the accumulation of L-lysine¹⁵. Moreover, Cg2612 shows high amino acid similarity with LOG proteins, suggesting that Cg2612 is possibly an LOG protein. In this report, in order to elucidate the function of Cg2612, we determined its crystal structure. Based on biochemical studies and structural comparison with other LOGs, we propose that Cg2612 functions as an LOG. In addition, we identified key residues responsible for enzyme catalysis and substrate binding.

Results

Overall structure of Cg2612. To investigate the function of Cg2612, we determined its crystal structure at a 2.3 Å resolution (Table 1). The asymmetric unit contained four molecules and seems to contain two distinct dimers. Molecules I, II, III, and IV of Cg2612 contain 9-191, 3-195, 3-190, and 2-195 residues visible in the electron density map, respectively. The R.M.S.D. values between these four monomeric structures are under 0.4, indicating that four monomers have quite similar structures each other. Interestingly, among four monomers in the asymmetric unit, two monomers contain a phosphate ion at each active site. We found that Lys194 from one dimer interacts with a phosphate in the active site of the other dimer (Supplementary Fig. S1). We speculate that crystal packing in I222 space group caused tetrameric arrangement as an artifact (Supplementary Fig. S1). Size-exclusion chromatography analysis suggested that Cg2612 forms a dimer (Supplementary Fig. S2). We then performed small-angle X-ray scattering (SAXS) experiment to further confirm the dimeric conformation of Cg2612 in solution, and the result indicates that Cg2612 functions as a dimer as observed in other LOGs (Supplementary Fig. S3).

The monomeric structure of Cg2612 shows an α/β fold belonging to a Rossmann fold (Fig. 1b,c). The central β -sheet which is formed by seven parallel β -strands is surrounded by eight α -helices (Fig. 1c). Dimerization of Cg2612 displays a compact domain folding. The dimerization interface is mainly composed of α 5- and α 6-helices, and the α 4-helix partially aids in dimerization (Fig. 1d and Supplementary Fig. S4). PISA¹⁶ computed the buried interface area to be 1,563 Å² (averaged with AB dimer and CD dimer) and the percentage of participating residues to be 24.5%. Dimerization of two polypeptides constitutes a pocket which serves as the active site, and the conserved "PGG_xGT_{xx}E" motif was found in the surface of the pocket, which will be described in detail later.

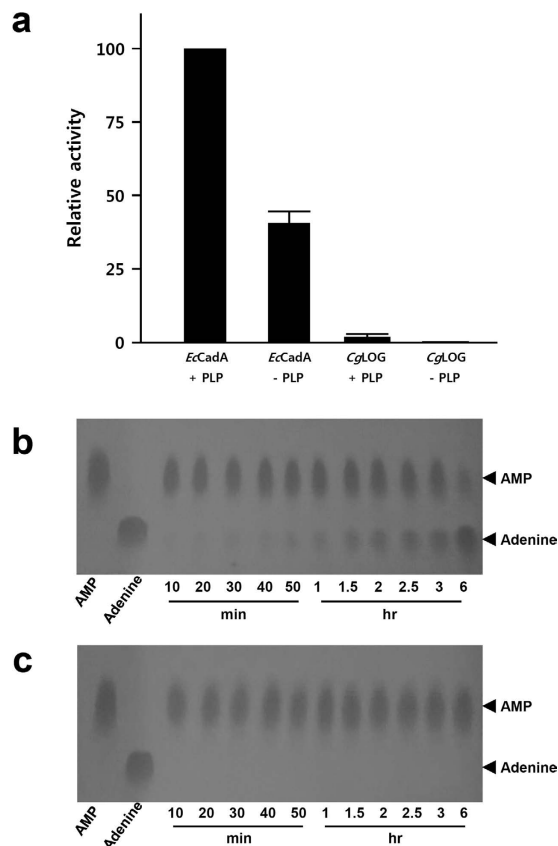


Figure 2. Phosphorobohydrolase activity of *CgLOG*. (a) Lysine decarboxylase activity assay of *EcCadA* and *CgLOG*. The lysine decarboxylase activity of *EcCadA* and *CgLOG* are measured with and without PLP. All experiments are performed in triplicates. (b,c) Phosphorobohydrolase activity of *EcCadA* (b) and *CgLOG* (c). The phosphorobohydrolase activity was detected by spotting and running the reaction mixture on TLC. The AMP and adenine standard are indicated. The incubation time of the reaction is labeled on the bottom of the figure.

***Cg2612* has LOG function.** Structural comparison using the DALI server¹⁷ showed that the structure of *Cg2612* is quite similar to LOG3 (*AtLOG3*, PDB CODE 2A33, Z-score 29.4) and LOG8 (*AtLOG8*, PDB CODE 1YDH, z-score 30.4) from *A. thaliana*. The comparison also showed that LOGs from *C. purpurea* (*CpLOG*, PDB CODE 5AJT, Z-score 26.8) and *M. marinum* (*MmLOG*, PDB CODE 3SBX, Z-score 27.7) are structural homologs of *Cg2612*. These structural homologs also shared amino acid identity higher than 33% with *Cg2612*. Because these structural homologs of *Cg2612* have been identified as LOG proteins, high similarity in structure and amino acid sequence with these proteins suggests that *Cg2612* functions as an LOG. To investigate the biochemical function of *Cg2612*, we performed lysine decarboxylase and phosphoribohydrolase activity assays on *Cg2612*, and compared the results with lysine decarboxylase from *E. coli* (*EcCadA*). As expected, *Cg2612* did not show any lysine decarboxylase activity, while *EcCadA* showed strong activity (Fig. 2a). These results indicate that *Cg2612* is not a lysine decarboxylase as inferred from previous studies on LOGs and high amino acid sequence identity of *Cg2612* with LOGs. We then tested if *Cg2612* has a phosphoribohydrolase activity. For this assay, we used adenosine monophosphate (AMP) as a substrate, because we could not obtain natural cytokinin precursors and it was previously reported that LOG has a phosphoribohydrolase activity against an AMP substrate⁹. Interestingly, we observed that *Cg2612* has phosphoribohydrolase activity and this activity tends to increase upon reaction time (Fig. 2b). However, LOGs generally show higher phosphoribohydrolase activity against natural cytokinin precursors than AMP^{5,9}, suggesting that *Cg2612* might have much higher phosphoribohydrolase activity against natural cytokinin precursors than observed with AMP as a substrate. On the other hand, *EcCadA* showed no phosphoribohydrolase activity with AMP as a substrate (Fig. 2c). These results confirm that *Cg2612* belongs to the LOG family, and hereafter, we will represent *Cg2612* as *CgLOG*.

Active site of *CgLOG*. In order to elucidate an active site and a substrate binding mode of *CgLOG*, we tried to determine the structure in complex with AMP or cytokinin. However, neither co-crystallization nor soaking of AMP or cytokinin into the *CgLOG* crystal was successful. We then superposed our structure with *MmLOG* in complex with AMP¹⁸. The active site of *CgLOG* is located near the “PGG_xGT_{xx}E” motif. The phosphate moiety was hydrogen bonded with main chains of Gly116, Ala117, and Gly118, and side chains of Thr119 and Ser19 (Fig. 3a). The ribose moiety is mainly stabilized by hydrogen bond interactions between Arg99 and two hydroxyl groups of the ribose moiety (Fig. 3a). To stabilize the adenine ring, a mixture of hydrophobic and hydrophilic

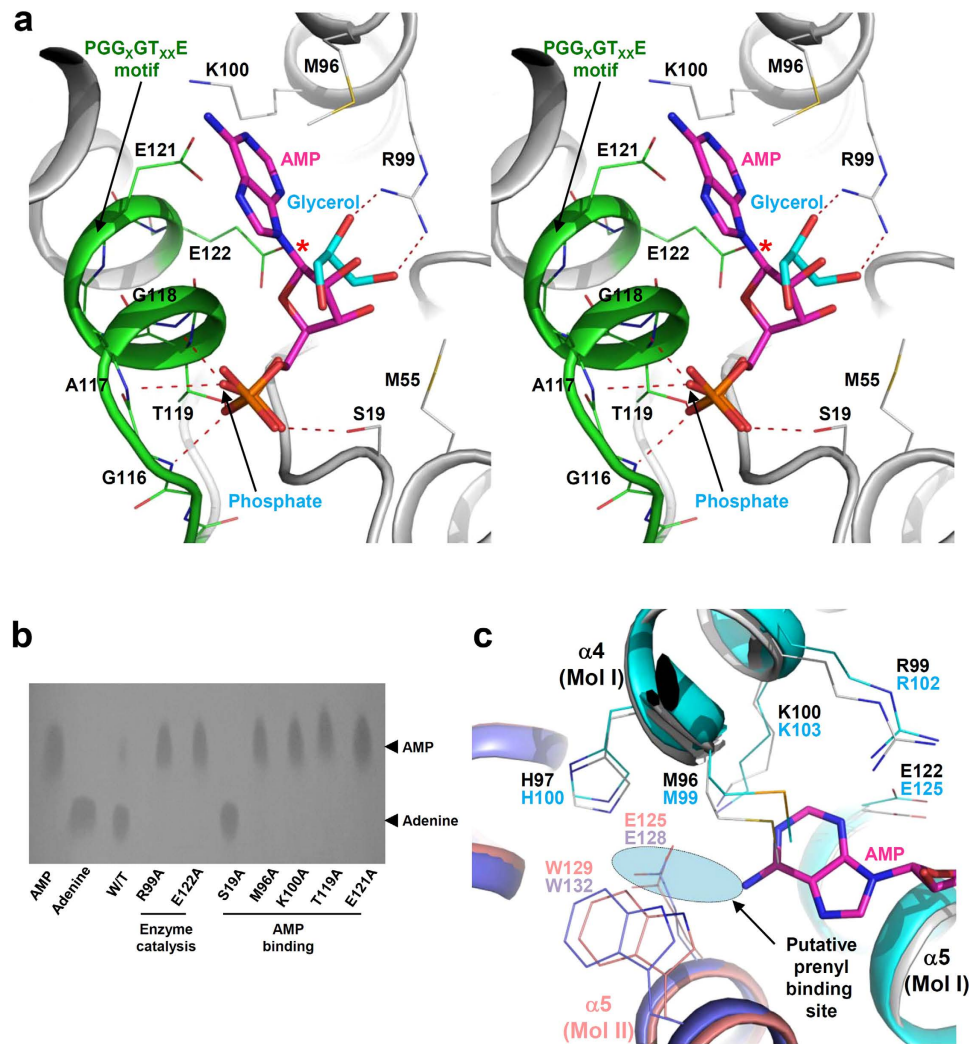


Figure 3. Active site of CgLOG. (a) Stereo view of the CgLOG AMP binding site. The CgLOG structure is superposed with LOG from *M. marinum* (MmLOG) in complex with AMP. The bound AMP molecule in MmLOG is shown with the CgLOG structure. Secondary structure elements are labeled. CgLOG is shown as a cartoon diagram. Residues involved in AMP binding are shown as line models. The bound AMP molecule was prepared as in Fig. 1b. The bound glycerol and phosphate molecules are labeled and shown as stick models. The hydrogen bonds involved in stabilization of the glycerol and phosphate molecules are shown with red dotted lines. The PGG_xGT_{xx}E motif is depicted with a green color. The covalent bond (a bond between adenine-N⁹ and ribose-C¹) hydrolyzed by the enzyme is indicated by a star symbol. (b) Site-directed mutagenesis experiments. The AMP and adenine standard are indicated. (c) Prenyl-group binding site. The CgLOG structure is superposed with AtLOG3. Two monomers of CgLOG are distinguished with colors of grey and salmon and those of AtLOG3 are with colors of cyan and light-blue. The bound AMP molecule is shown as a stick model in magenta. Two catalytic residues (R39 and E122 in CgLOG) and residues involved in the constitution of the prenyl-group binding site are shown as line models. The putative prenyl-group binding site is labeled and shown with a cyan circle.

residues, Met96, Lys100, and Glu121, form an adenine binding site (Fig. 3a). Two proposed catalytic residues, Arg99 and Glu122, are located in the vicinity of the bond to be hydrolyzed; a covalent bond between adenine-N⁹ and ribose-C¹ (Fig. 3a). Among the residues involved in AMP binding and enzyme catalysis, Gly116, Ala117, Gly118, Thr119, Glu121, and Glu122 are located in the “PGG_xGT_{xx}E” motif, indicating that the motif serves as a nucleotide binding site as suggested by other LOG structures. In our current structure, one phosphate and one glycerol molecule are bound at the AMP binding site and these molecules mimic the stabilization of the phosphate moiety and the ribose ring, respectively (Fig. 3a and Supplementary Fig. S5). In order to confirm the involvement of these residues in AMP binding and enzyme catalysis, we performed site-directed mutagenesis experiments. As expected, substituting these crucial residues with alanines resulted in almost complete loss of phosphoribohydrolase activity (Fig. 3b). One exception is S19A mutant which shows higher activity than the wild-type. Most of the residues that involved in AMP stabilization are conserved in all LOGs, and the active site

conformation observed in CgLOG further supports the classification of this protein as a LOG family enzyme (Fig. 1b).

Stabilization of the prenyl-group, the N⁶-modifying moiety of cytokinin precursors, still remains unclear due to the absence of a LOG structure in complex with a natural substrate or cytokinin. However, the binding site of the N⁶-prenyl group could be inferred from configuration of the adenine moiety and positioning of N⁶ atom of AMP bound in *Mm*LOG. Superposition of the CgLOG structure with *Mm*LOG in complex with AMP also leads us to speculate the prenyl-group binding site of CgLOG. In CgLOG, Met96, His97, Lys100, Glu125, and Trp129 seem to form a prenyl-group binding site (Fig. 3c). The prenyl-group binding locates at the dimer interface and especially Glu125 and Trp129 residues are provided from a neighboring molecule (Fig. 3c). Importantly, these residues are identical to those found in *At*LOG3, *Os*LOG, and *Cp*LOG (Figs 1b and 3c). Based on these observations, we propose that CgLOG utilizes cytokinin precursors as substrates that are similarly used by other LOGs from plants or plant-interacting fungus.

Structural comparison of CgLOG with other LOGs. To compare CgLOG with other LOGs, we superposed the CgLOG structure with other LOG proteins such as *At*LOG3, *Cp*LOG, and *Mm*LOG. Although the overall folds of all four LOG structures are quite similar to each other, *Cp*LOG exhibited somewhat unique structural features. Compared with the three other LOGs, *Cp*LOG has an extra helix in the C-terminal region and contains extended connecting loops of α 3- β 4 and α 4- β 5 (Fig. 4a). Notably, the extended connecting loop of α 3- β 4 is located near the AMP binding site (Fig. 4a). In *At*LOG3 this region is distorted, in CgLOG this region showed high a b-factor. However, in *Mm*LOG, this region contains the Glu80 residue that forms direct a hydrogen bond with the hydroxyl group of the ribose ring (Fig. 4b). These observations indicate that this region is quite diverse in various LOGs and stabilization of the ribose ring seems to occur somewhat differently in each protein. Except for structural differences in this region, LOGs have similar AMP binding modes (Fig. 4b). The conserved residues in “PGG_xGT_{xx}E” motifs along with other conserved residues contribute to AMP stabilization (Figs 1b and 4b and Supplementary Fig. S6). One exception is found in *Mm*LOG; Ala19 and Asp120 are involved in AMP stabilization while serine and glutamate residues are located at the corresponding positions in other LOGs (Fig. 4b). Moreover, all four LOGs have two catalytic residues, and Arg99 and Glu122 in CgLOG are located at the same positions, indicating that these LOGs catalyze this reaction via the same catalytic mechanism. The comparison of the prenyl-group binding sites provides insights into LOG substrate specificity. As observed in CgLOG, *At*LOG3 and *Cp*LOG contain the residues Met96, His97, Lys100, Glu125, and Trp129 at the prenyl-group binding site (Fig. 4c). However, *Mm*LOG has a glaring discrepancy in the prenyl-group binding site compared with CgLOG, *At*LOG3, and *Cp*LOG. At the prenyl-group binding site in *Mm*LOG, Asp124, Glu128, and Trp96 residues are located at the positions corresponding to glutamate, tryptophan, and histidine residues, respectively, in the other three LOGs (Fig. 4c). These comparisons suggest that CgLOG might produce cytokinins similar to those produced by LOGs from plants and plant-interacting fungi. However, *Mm*LOG might produce different types of cytokinins than CgLOG, *At*LOG3 and *Cp*LOG, which drives us to speculate that mammalian-interacting bacteria like those in the *Mycobacterium* genus seem to utilize different types of cytokinins.

Discussion

Our structural and biochemical studies on Cg2612, a protein previously annotated as a LDC, imply that this protein functions as LOG. Because LOGs are enzymes that catalyze the production of cytokinins, here we can raise the question if *C. glutamicum* truly synthesizes cytokinins. As we mentioned above, the first reaction for cytokinin production is the prenylation of ATP/ADP/AMP or tRNA by IPTs, and these enzymes can be divided into two categories depending on whether they utilize nucleotides or tRNA as a substrate. Adenylate-IPT is usually found in higher plants or phytopathogens (known as *Fas4*) as a main regulator for cytokinin levels, while tRNA-IPT (*MiaA*) is ubiquitous to improve the efficiency and fidelity of the codon-anticodon interaction during translation¹⁹. It was reported that *M. tuberculosis* H37Rv produces cytokinins such as iP and tZ⁹. Interestingly, genome analysis of *M. tuberculosis* H37Rv revealed that this strain contains a gene coding for tRNA-IPT (*Rv2727c*, *LH5714920*, *MiaA*), but not for adenylate-IPT. This analysis intimated that the tRNA-mediated cytokinin activation is a major pathway for cytokinin production in bacteria, although it was considered to be a minor pathway in *Arabidopsis*²⁰. Like *M. tuberculosis*, the genome of *C. glutamicum* ATCC 13032 only contains a gene coding for tRNA-IPT (*Cg2130*, *MiaA*). In addition, Cg2130 exhibits 56.9% amino acid sequence identity with *Rv2727c*. These results indicate that *C. glutamicum* seems to produce cytokinins by a tRNA-mediated activation mechanism similar to the mechanism in *M. tuberculosis*. Thus, studies on cytokinin detection and biosynthesis in *C. glutamicum* are needed.

Some soil bacteria communicate with plants via cytokinins. For instance, *Rhodococcus fascians* produces cytokinins to infect a wide range of plants and causes diseases in plant hosts such as a leafy gall syndrome²¹. The virulence of *C. glutamicum* in plant species has not yet been reported. However, because *C. glutamicum* is a soil-dwelling bacterium in nature, investigating *C. glutamicum*-plant communication through cytokinins is of interest for agricultural applications. Furthermore, recent studies on cytokinin production in *M. tuberculosis*, a mammalian pathogen, suggest that cytokinin production by microbes is not limited to communication with plants, but rather can be applied to wide cross-kingdom communications^{9,22}.

Methods

Protein preparations. The gene coding for LOG from *Corynebacterium glutamicum* ATCC 13032 (CgLOG) was amplified from chromosome of *C. glutamicum* by polymerase chain reaction (PCR) with primers: forward, 5-GCGCCATATGACTTCGCTTTTCGACGCC-3, and reverse, 5-GCGCCTCGAGCCATTTTGGTGCTGGTGGAGTCC-3. The PCR product was then subcloned into pET30a (Novagen) with 6xHis at the C-terminus. The resulting expression vectors pET30a: CgLOG was transformed into

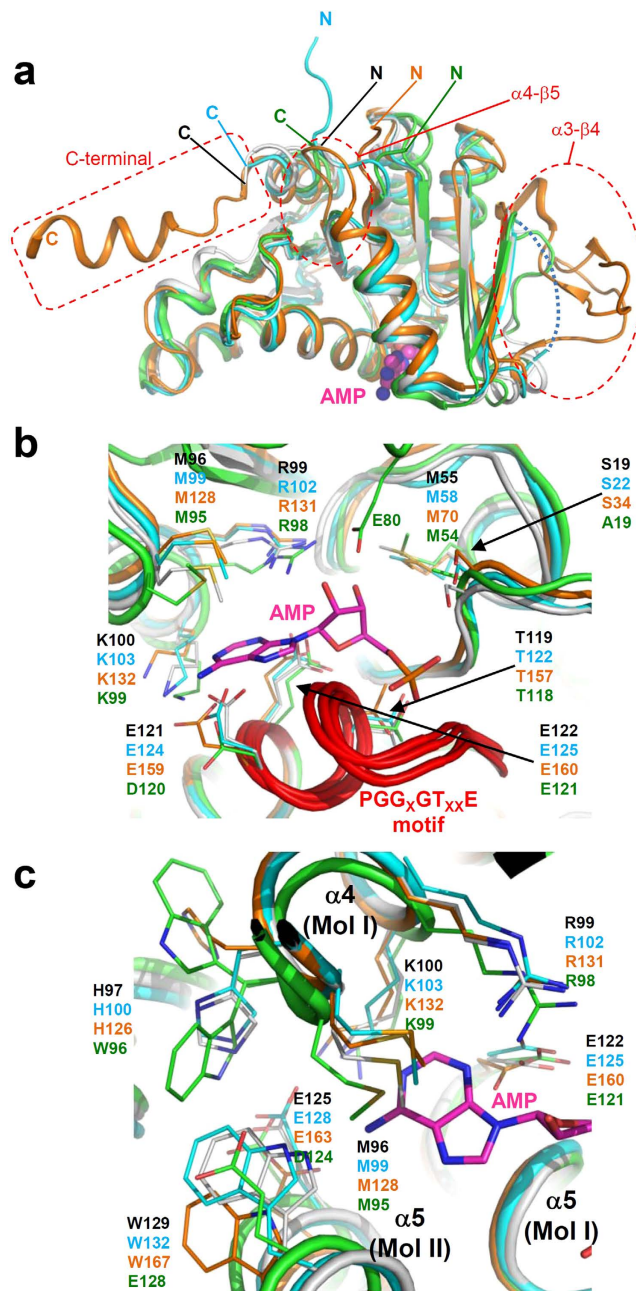


Figure 4. Structural comparison of CgLOG with other LOGs. (a) Comparison of overall structure. Monomeric structures of CgLOG, AtLOG, CpLOG, and MmLOG are superposed and presented as cartoon diagrams in grey, cyan, orange, and green, respectively. The AMP molecule bound in the MmLOG structure is shown in magenta as a stick model. The N-terminus and the C-terminus of LOGs are indicated. Structural differences found in CpLOG are indicated with red dotted circles and labeled. The distorted connecting loop of $\alpha 3\text{-}\beta 4$ in AtLOG3 is shown with a cyan dotted line. (b) Structural comparison in AMP binding sites. Monomeric structures of CgLOG, AtLOG, CpLOG, and MmLOG are superposed and presented with color scheme as in (a). Residues of four LOGs involved in AMP binding are shown as line models and labeled with the same color scheme as in (a). The "PGG_xGT_{xx}E" motifs of LOGs are distinguished with a red color and labeled. (c) Structural comparison of prenyl-group binding sites. Dimeric structures of CgLOG, AtLOG, CpLOG, and MmLOG are superposed and presented with color scheme as in (a). Residues of four LOGs involved in the constitution of the putative prenyl-group binding site are shown as line models and labeled with the same color scheme as in (a).

E. coli BL21 (DE3) strain and was grown on LB medium containing 100 mg l⁻¹ kanamycin at 37 °C to OD600 of 0.6. After induction with 1.0 mM 1-thio- β -D-galactopyranoside (IPTG) for a further 20 h at 18 °C, the culture was harvested by centrifugation at 5,000 \times g for 15 min at 4 °C. The cell pellet was resuspended in ice-cold buffer

A (40 mM Tris-HCl, pH 8.0) and disrupted by ultrasonication. The cell debris was removed by centrifugation at $11,000 \times g$ for 1 h, and lysate was bound to Ni-NTA agarose column (Qiagen). After washing with buffer A containing 20 mM imidazole, the bound proteins were eluted with 300 mM imidazole in buffer A. Further purification was carried out by applying the HiTrap Q ion exchange chromatography and size exclusion chromatography. The purified proteins were concentrated to 30 mg ml^{-1} in 40 mM Tris-HCl, pH 8.0, and stored at -80°C for crystallization trials. Site-directed mutagenesis experiments were performed using the QuikChange site-directed mutagenesis kit (Stratagene). The production and purification of the CgLOG mutants were carried out by the same procedures as described for the wild-type protein. CadA from *E. coli* (EcCadA) was prepared by the procedure similar to CgLOG.

Crystallization, data collection and structure determination. Crystallization of the purified proteins were initially performed by the hanging-drop vapor-diffusion method at 20°C using commercially available sparse-matrix screens from Hampton Research and Emerald BioSystems. Each experiment consisted of mixing $1.0 \mu\text{l}$ protein solution with $1.0 \mu\text{l}$ reservoir solution and then equilibrating it against 0.5 ml of the reservoir solution. The CgLOG crystals were observed from several crystallization screening conditions. After several optimization steps using the hanging-drop vapor-diffusion method, the best-quality crystals appeared in 2 day using a reservoir solution consisting of 0.2 M DL-malic acid, pH 7.0 and 24% PEG 3350 and reached maximal dimensions of approximately $0.3 \times 0.3 \times 0.1 \text{ mm}$. For the cryo-protection of the crystals, glycerol of 30% glycerol in reservoir solution was used. Data were collected at the 7A beamline at the Pohang Accelerator Laboratory using a QUANTUM 270 CCD detector (San Diego, CA, USA) at the wavelength of 0.97934 \AA . The CgLOG crystal diffracted to resolution of 2.3 \AA . The data was then indexed, integrated, and scaled using the HKL2000 program²³. Crystals of CgLOG belonged to the I-centered orthorhombic space group *I*222 with unit cell dimensions of $a = 113.51 \text{ \AA}$ $b = 130.50 \text{ \AA}$ $c = 140.51 \text{ \AA}$. With four CgLOG molecules per asymmetric unit, the crystal volume per unit of protein mass was approximately $3.10 \text{ \AA}^3 \text{ Da}^{-1}$, which corresponds to a solvent content of approximately 60.31%²⁴. The structure of CgLOG was solved by molecular replacement method using *MOLREP*²⁵ with LOG from *A. thaliana* (AtLOG, PDB CODE 2A33) as a search model. The model building was performed using the program *WinCoot*²⁶ and the refinement was performed with *REFMAC5*²⁷. The data statistics are summarized in Table 1. The refined models of CgLOG was deposited in the Protein Data Bank (PDB CODE 5ITS).

Solution SAXS measurements. Small-angle X-ray scattering (SAXS) measurements were carried out using the 4C SAXS II beamline of the Pohang Accelerator Laboratory (Pohang, Korea). A sample-to-detector distance (SDD) of 4.00 m and 1.00 m for SAXS were used. The magnitude of scattering vector, $q = (4\pi/\lambda) \sin \theta$, was $0.1 \text{ nm}^{-1} < q < 6.50 \text{ nm}^{-1}$, where 2θ is the scattering angle and λ is the wavelength of the X-ray beam source. All scattering measurements were carried out at 4°C by using a FP50-HL refrigerated circulator (JULABO, Germany). The SAXS data were collected in six successive frames of 0.1 min each to monitor radiation damage. Measurements of CgLOG were carried out over a small concentration range $0.5 \sim 4.5 \text{ mg/ml}$. Each 2D SAXS pattern was radial averaged from the beam center and normalized to the transmitted X-ray beam intensity, which was monitored with a scintillation counter placed behind the sample. The $R_{g,G}$ (radius of gyration) values were estimated from the scattering data using Guinier analysis²⁸. The molecular mass (MM) was calculated from the scattering curve based on the Q_R method²⁹. The pair distance distribution $p(r)$ function was obtained through the indirect Fourier transform method using the program GNOM³⁰.

Lysine decarboxylase activity assay. The activity of LDC was determined by measuring residual concentration of L-lysine using lysine oxidase and peroxidase. After LDC reaction, lysine oxidase converts remaining lysine into 6-amino-2-oxohexanoate, NH_3 , and H_2O_2 and then the hydrogen peroxide is reduced by peroxidase with 2,2'-azino-bis(3-ethylbenzothiazoline-6-sulphonic acid) (ABTS). The oxidized ABTS is detected by spectrophotometric method in absorbance at 412 nm. The assay was performed at 30°C in a total volume $200 \mu\text{l}$, containing 100 mM potassium phosphate, pH 6.0, 0.1 M L-lysine, 0.2 mM pyridoxal-5-phosphate, and $25 \mu\text{g}$ of purified enzymes. The reaction was stopped by heating the reaction mixture at 100°C for 5 min. After centrifugation at $13,500 \times g$ for 1 min, 2X reaction solution that contains 0.1 unit ml^{-1} lysine oxidase and 1 unit ml^{-1} peroxidase in potassium phosphate buffer is added to the reaction mixture.

Phosphoribohydrolase activity assay. The phosphoribohydrolase activity was determined by detecting adenine ring compounds separated by thin layer chromatography (TLC) method. Enzyme reactions were carried out in the mixture of 20 mM AMP, 36 mM Tris-HCl, pH 8.0, and $23 \mu\text{M}$ purified enzymes at 30°C and then the reactions were stopped by heating the mixture at 95°C for 1.5 min. The reaction mixtures were then dotted on PEI-cellulose-F plastic TLC sheet (Merck Millipore). The mobile phase was 1 M sodium chloride. After development in the TLC chamber, the sheet was dried completely. Adenine ring-including compounds were detected by UV lamp (290 nm).

Size-exclusion chromatographic analysis. To investigate the oligomerization of CgLOG, analytical size-exclusion chromatography was performed using a Superdex 200 10/300 column (GE Healthcare) at NaCl concentrations of 150 mM. $300 \mu\text{L}$ of protein samples with concentration of 3 mg/ml were analyzed. The molecular weights of the eluted samples were calculated based on the calibration curve of standard samples.

References

1. Skoog, F. & Armstrong, D. J. Cytokinins. *Annual review of plant physiology* **21**, 359–384 (1970).
2. Sakakibara, H. Cytokinins: activity, biosynthesis, and translocation. *Annu Rev Plant Biol* **57**, 431–49 (2006).
3. Mok, D. W. & Mok, M. C. Cytokinin Metabolism and Action. *Annu Rev Plant Physiol Plant Mol Biol* **52**, 89–118 (2001).

4. Kakimoto, T. Identification of plant cytokinin biosynthetic enzymes as dimethylallyl diphosphate: ATP/ADP isopentenyltransferases. *Plant and Cell Physiology* **42**, 677–685 (2001).
5. Hinsch, J. *et al.* De novo biosynthesis of cytokinins in the biotrophic fungus *Claviceps purpurea*. *Environmental microbiology* (2015).
6. Kurakawa, T. *et al.* Direct control of shoot meristem activity by a cytokinin-activating enzyme. *Nature* **445**, 652–5 (2007).
7. Kukimoto-Niino, M. *et al.* Crystal structures of possible lysine decarboxylases from *Thermus thermophilus* HB8. *Protein Sci* **13**, 3038–42 (2004).
8. Kuroha, T. *et al.* Functional analyses of LONELY GUY cytokinin-activating enzymes reveal the importance of the direct activation pathway in *Arabidopsis*. *Plant Cell* **21**, 3152–69 (2009).
9. Samanovic, M. I. *et al.* Proteasomal control of cytokinin synthesis protects *Mycobacterium tuberculosis* against nitric oxide. *Mol Cell* **57**, 984–94 (2015).
10. Jeon, W. B. *et al.* X-ray crystal structures of the conserved hypothetical proteins from *Arabidopsis thaliana* gene loci At5g11950 and AT2g37210. *Proteins* **65**, 1051–4 (2006).
11. Dzurowa, L. *et al.* The three-dimensional structure of “Lonely Guy” from *Claviceps purpurea* provides insights into the phosphoribohydrolase function of Rossmann fold-containing lysine decarboxylase-like proteins. *Proteins* **83**, 1539–46 (2015).
12. Vertes, A. A., Inui, M. & Yukawa, H. Manipulating corynebacteria, from individual genes to chromosomes. *Appl Environ Microbiol* **71**, 7633–42 (2005).
13. Hayashi, M. *et al.* Transcriptome analysis reveals global expression changes in an industrial L-lysine producer of *Corynebacterium glutamicum*. *Bioscience, biotechnology, and biochemistry* **70**, 546–550 (2006).
14. Purich, D. L. & Allison, R. D. *The enzyme reference: a comprehensive guidebook to enzyme nomenclature, reactions, and methods* (Academic press, 2003).
15. Kalinowski, J. *et al.* The complete *Corynebacterium glutamicum* ATCC 13032 genome sequence and its impact on the production of L-aspartate-derived amino acids and vitamins. *J Biotechnol* **104**, 5–25 (2003).
16. Krissinel, E. & Henrick, K. Inference of macromolecular assemblies from crystalline state. *Journal of molecular biology* **372**, 774–797 (2007).
17. Holm, L. & Sander, C. Touring protein fold space with Dali/FSSP. *Nucleic Acids Res* **26**, 316–9 (1998).
18. Baugh, L. *et al.* Increasing the structural coverage of tuberculosis drug targets. *Tuberculosis (Edinb)* **95**, 142–8 (2015).
19. Persson, B., Esberg, B., Olafsson, O. & Björk, G. Synthesis and function of isopentenyl adenosine derivatives in tRNA. *Biochimie* **76**, 1152–1160 (1994).
20. Miyawaki, K. *et al.* Roles of *Arabidopsis* ATP/ADP isopentenyltransferases and tRNA isopentenyltransferases in cytokinin biosynthesis. *Proceedings of the National Academy of Sciences* **103**, 16598–16603 (2006).
21. Stes, E., Vandeputte, O. M., El Jaziri, M., Holsters, M. & Vereecke, D. A successful bacterial coup d'état: how *Rhodococcus fascians* redirects plant development. *Annu Rev Phytopathol* **49**, 69–86 (2011).
22. Naseem, M., Sarukhanyan, E. & Dandekar, T. LONELY-GUY Knocks Every Door: Crosskingdom Microbial Pathogenesis. *Trends Plant Sci* (2015).
23. Otwinowski, Z. & Minor, W. Processing of X-ray diffraction data collected in oscillation mode. *Methods Enzymol* **276**, 307–326 (1997).
24. Matthews, B. W. Solvent content of protein crystals. *Journal of molecular biology* **33**, 491–497 (1968).
25. Vagin, A. & Teplyakov, A. Molecular replacement with MOLREP. *Acta Crystallographica Section D: Biological Crystallography* **66**, 22–25 (2009).
26. Emsley, P. & Cowtan, K. Coot: model-building tools for molecular graphics. *Acta Crystallographica Section D: Biological Crystallography* **60**, 2126–2132 (2004).
27. Murshudov, G. N., Vagin, A. A. & Dodson, E. J. Refinement of macromolecular structures by the maximum-likelihood method. *Acta Crystallographica Section D: Biological Crystallography* **53**, 240–255 (1997).
28. Glatter, O. & Kratky, O. *Small angle X-ray scattering* (Academic press, 1982).
29. Rambo, R. P. & Tainer, J. A. Accurate assessment of mass, models and resolution by small-angle scattering. *Nature* **496**, 477–481 (2013).
30. Semenyuk, A. & Svergun, D. GNOM—a program package for small-angle scattering data processing. *Journal of Applied Crystallography* **24**, 537–540 (1991).

Acknowledgements

This work was supported by a National Research Foundation of Korea (NRF) grant funded by the Korean Government (MSIP) (2014R1A2A2A01005752 and 2014M1A2A2033626), and was also supported by the New & Renewable Energy Core Technology Program of the Korea Institute of Energy Technology Evaluation and Planning (KETEP) granted financial resource from the Ministry of Trade, Industry & Energy, Republic of Korea (No. 20153030091360).

Author Contributions

H.S. and K.-J.K. designed the project. H.S., S.K., H.-Y.S., I.-K.K. and H.F.S. performed the experiments. K.S.J. performed and analyzed the SAXS measurements. H.S. and K.-J.K. wrote the paper.

Additional Information

Supplementary information accompanies this paper at <http://www.nature.com/srep>

Competing financial interests: The authors declare no competing financial interests.

How to cite this article: Seo, H. *et al.* Structural basis for cytokinin production by LOG from *Corynebacterium glutamicum*. *Sci. Rep.* **6**, 31390; doi: 10.1038/srep31390 (2016).



This work is licensed under a Creative Commons Attribution 4.0 International License. The images or other third party material in this article are included in the article's Creative Commons license, unless indicated otherwise in the credit line; if the material is not included under the Creative Commons license, users will need to obtain permission from the license holder to reproduce the material. To view a copy of this license, visit <http://creativecommons.org/licenses/by/4.0/>

© The Author(s) 2016